Functional ultrasound imaging to study brain dynamics: Application of pharmaco-fUS to atomoxetine

Benjamin Vidal, Marine Droguerre, Ludovic Venet, Luc Zimmer, Marco Valdebenito, Franck Mouthon, Mathieu Charvériat

Functional ultrasound imaging to study brain dynamics: Application of pharmaco-fUS to atomoxetine

Benjamin Vidal [a,b,*,1], Marine Droguerre [a,1], Ludovic Venet [a], Luc Zimmer [b,c,d], Marco Valdebenito [c], Franck Mouthon [a], Mathieu Charvériat [a]

[a] *Theranexus, Lyon, France*
[b] *Lyon Neuroscience Research Center, Bron, France*
[c] *CERMEP-Université Lyon 1, Lyon, France*
[d] *Hospices Civils de Lyon, Lyon, France*

A R T I C L E I N F O

Keywords:
Pharmaco-fUS
Atomoxetine
Functional ultrasound imaging

A B S T R A C T

Functional ultrasound (fUS) is a new tool enabling the imaging of brain activity through the regional monitoring of cerebral blood volume (CBV) dynamics. This innovative technique has not yet demonstrated its full potential in pharmacological applications and drug development. In the current proof-of-concept study, the impact of atomoxetine (ATX), a potent norepinephrine reuptake inhibitor and non-stimulant treatment marketed in attention-deficit/hyperactivity-disorder, was evaluated in anesthetized rat using pharmacological functional ultrasound (pharmaco-fUS) at increasing doses (0.3, 1 and 3 mg/kg). Using regions of interest (acute changes of CBV and functional connectivity) or pixel-based (general linear modeling and independent component analysis) analysis, we here demonstrated that ATX consistently displayed a hemodynamic effect in the visual cortex, the dentate gyrus and thalamus, especially visual areas such as lateral posterior thalamic nuclei and lateral geniculate nuclei (LGN). The time profile of ATX effects was dose-dependent, with fastest CBV increases at the highest dose, and longer CBV increases at the intermediate dose. Standardizing the use of pharmaco-fUS could improve our understanding of the mechanism of action of drugs active in the brain and might constitute a new step to move forward in drug development for neurological disorders.

1. Introduction

Functional neuroimaging refers to diverse *in vivo* brain imaging modalities and classically to functional Magnetic Resonance Imaging (fMRI) and Positron Emission Tomography (PET). Both allow molecular and functional exploration and are widely used in non-clinical and clinical studies. However, the last few years have seen the emergence of a new neuroimaging tool, functional Ultrasound (fUS) (Mace et al., 2011), able to locally monitor cerebral blood dynamics. Based on ultrasonic plane wave emissions, fUS allows the capture of more than 20, 000 frames per second, boosting the power Doppler signal-to-noise ratio (up to 50 compared to conventional Doppler ultrasound techniques) and thus enhancing the temporal resolution compared to fMRI and PET (~400 ms for fUS; ~2 s for fMRI and several minutes for PET - see Catana, 2019; Mandino et al., 2019; Urban et al., 2017 for review). Unlike conventional Doppler ultrasound, cerebral blood volume (CBV) measurements using fUS are achievable in microvasculature such as arterioles and venules, even in the deepest brain areas (Blaize et al., 2020; Mace et al., 2011), with an excellent spatial resolution (~100 μm) in comparison to fMRI and PET (~300–400 μm and 1–2 mm, respectively - (Lancelot and Zimmer, 2010; Logothetis, 2008)). In rodents, applications of fUS technique were demonstrated for sensory signal processing either after visual (Gesnik et al., 2017; Mace et al., 2018), olfactory (Osmanski et al., 2014), forepaw (Urban et al., 2014) or whiskers (Mace et al., 2011) stimulations. Apart from rodents, different species have been evaluated using fUS, such as birds (Rau et al., 2018), rabbits (Kohlhauer et al., 2015), ferrets (Bimbard et al., 2018), non-human primates (Dizeux et al., 2019) and humans (Demene et al., 2017; Imbault et al., 2017). To the best of our knowledge, this technology has not yet fully demonstrated its potential as a tool to characterize central effects of systemic administrations of central nervous system (CNS) drugs, despite a previous study on pharmacological

* Corresponding author. 59 Boulevard Pinel, 69677, Bron, France.
E-mail address: benjamin.vidal@theranexus.fr (B. Vidal).
[1] Both authors contributed equally.

stimulation by local injections of 4-aminopyridine in rat brain to induce epileptiform seizures (Mace et al., 2011).

To highlight the potential of this neuroimaging tool, we selected atomoxetine (ATX), a norepinephrine (NE) reuptake transporter (NET) inhibitor (Bymaster et al., 2002; Gehlert et al., 1995; Tatsumi et al., 1997), and the first non-stimulant prescribed treatment for patients with Attention Deficit Hyperactivity Disorder (ADHD) (Pliszka, 2003; Walker et al., 2015). ATX improves various executive functions in patient with ADHD (Brown et al., 2011; Cubillo et al., 2014; Gau and Shang, 2010; Walker et al., 2015) and reduces both impulsivity in wild-type rats and locomotor hyperactivity in different animal models of ADHD (Arime et al., 2011; Fernando et al., 2012). A pre-clinical fMRI study (Easton et al., 2007) revealed that ATX administration was associated with changes in brain regions associated with the caudate putamen, cortico-basal thalamic loop circuits and other behavioral control areas, underlining the relevance of the use of this drug in ADHD. Thus, in the present study and as proof of concept, we investigated the pharmacological effect of ATX, on CBV responses using fUS in anesthetized rats.

2. Materials and methods

2.1. Animals

Fifteen Wistar-Kyoto (8-week old) male rats were used in the study, that were purchased from Janvier labs (France) and maintained under controlled environmental conditions (12/12 h light-dark cycle, light on at 7 a.m., 22 ± 1 °C ambient temperature, 60% relative humidity) with food and water *ad libitum*. Animal surgery and experimentations were conducted in strict accordance with the recommendations and guidelines of the European Union (Directive 2010/63/EU) and strictly followed the policies of the French ethic committee for preclinical research. Procedures and protocols herein described were authorized by the French Ministry of Research (authorization reference: APAFIS19829). All efforts were made to improve animal welfare and minimize animal sufferings.

2.2. Drugs and administration procedures

Atomoxetine (Sigma-Aldrich) was dissolved in saline and administered intraperitoneally (2 mL/kg) at 0.3 (n = 4), 1 (n = 3) and 3 mg/kg (n = 4). For the control group, only saline was administered at the same volume (n = 4).

2.3. Functional ultrasound imaging

One day prior to ultrasound imaging, a thin-skulled surgery was performed under isoflurane (4% in 1 L/min) and with buprenorphine (0.05 mg/kg; (Buprecare, Axience)) pretreatment. After shaving and cleaning with betadine, the scalp was incised and the skin was pulled in order to visualize the lateral sides of the skull from the bregma to the lambda anatomical landmarks. The bone was thinned from −3.00 mm to −7.00 mm (AP) and +5.00 to −5.00 mm (L) from bregma using a drill at low speed with a micro drill steel burr (Harvard Apparatus, 75–1887). Saline was frequently added between drilling sessions to avoid overheating until the skull was thin enough to be flexible. The scalp was then sutured, betadine and lidocaine were locally applied and the rats were allowed to recover from anesthesia. During fUS imaging procedure, rats were maintained under anesthesia with isoflurane (2%). A catheter was placed intraperitoneally for pharmacological injection during the scan. The rats were then placed in a stereotaxic frame. The body temperature was rectally monitored and maintained using a heating blanket, and respiratory and heart rates were also continuously monitored (TCMT, Minerve, France). The thinned skull was covered with ultrasound gel. The rats were scanned with a prototype system dedicated to small animal ultrasound neuroimaging (Iconeus, Paris, France). Doppler vascular images were obtained using the Ultrafast Compound Doppler Imaging technique (Bercoff et al., 2011). Each frame was a Compound Plane Wave frame (Montaldo et al., 2009) resulting from the coherent summation of backscattered echoes obtained after successive tilted plane waves emissions. A stack of hundreds of such compounded frames was acquired with very high frame rate. Then, the blood volume signal was extracted from the tissue signal by filtering the image stacks with a dedicated spatiotemporal filter using Singular Value Decomposition (Demene et al., 2015). Each transcranial Doppler image was obtained from 200 compounded frames acquired at 500 Hz frame rate. A fast-anatomical scan with successive images taken on several coronal planes was first performed to identify the vascular landmarks for further positioning of the probe, as previously described (Tiran et al., 2017). For fUS imaging acquisitions, a Doppler image was acquired every second during 15 min at bregma −5.3 mm (Fig. 1a and b). The pharmacological challenge was performed at 5 min by injection of atomoxetine or saline.

2.4. Data analysis

2.4.1. Analysis on the regions of interest

For each scan, the regions of interest (visual cortex, retrosplenial cortex, LGN, hippocampus, superior colliculus, thalamus, and midbrain) were manually assigned according to the stereotaxic atlas of the rat brain (Paxinos and Watson, 1998), as shown in Fig. 1c, and the CBV time courses were extracted. The signal was expressed as percentage of the baseline and averaged between the scans (Fig. 1e). The mean CBV changes were calculated for the first 5 min after injection, for each region. In the same time period, we also determined the maximal CBV increase, Emax, and its corresponding time point, Tmax (Fig. 2a and b).

A functional connectivity analysis was also performed. After low-pass filtering (cut-off frequency of 0.2 Hz) and removal of linear trend calculated from the baseline, the temporal CBV correlations were measured by the Pearson correlation coefficient for each pair of regions from 0 to 5 min (baseline period) and from 5 to 15 min (post-injection period). For each condition, the connectivity changes occurring after injection were calculated by the difference of correlation coefficients [post-injection - baseline] (Fig. 2c).

2.4.2. Pixel-based analysis

Pixel-based analysis was performed using several modeling and preprocessing approaches. The first approach (Fig. 3a) used spatial preprocessing and statistical comparisons across time-bins with the software SPM12 (Wellcome Trust Center for Neuroimaging, London, UK). In the preprocessing, all images were automatically realigned together and an isotropic Gaussian filter was applied (0.4 × 0.4 × 0.4 mm^3 Full Width at Half Maximum (FWHM), with a spatial resolution of 100 × 100 × 400 μm^3). A first-level analysis was performed on each scan using a flexible factorial dividing the scan into three time-bins of 5 min each. The first-level parametric contrast images (comparing the post-injection time-bins with the baseline) were then used in the second-level analysis, enabling to quantify at the group level the CBV changes after injection of atomoxetine as compared to the vehicle injection.

The second approach (Fig. 3b) used the same statistical analysis, after a denoising step was added in the preprocessing, based on individual independent component analysis (ICA) of each scan (Fig. 3c). After the realignment step, the ICA analysis was carried out using FSL software (FMRIB's Software Library). A high-pass temporal filter was applied to the data and a cut-off frequency of 0.0067 Hz; the Probabilistic Independent Component Analysis (Beckmann and Smith, 2004) was performed in MELODIC Version 3.15. The following data pre-processing was applied to the input data: pixel-wise de-meaning of the data; normalization of the pixel-wise variance. Pre-processed data were whitened (*i.e.*, corrected for temporal autocorrelation) and projected into a 25-dimensional subspace using Principal Component Analysis. The corrected data were decomposed into sets of vectors which supported signal variation across the temporal domain (time-courses) and spatial (maps) domains (Hyvarinen, 1999). Components were

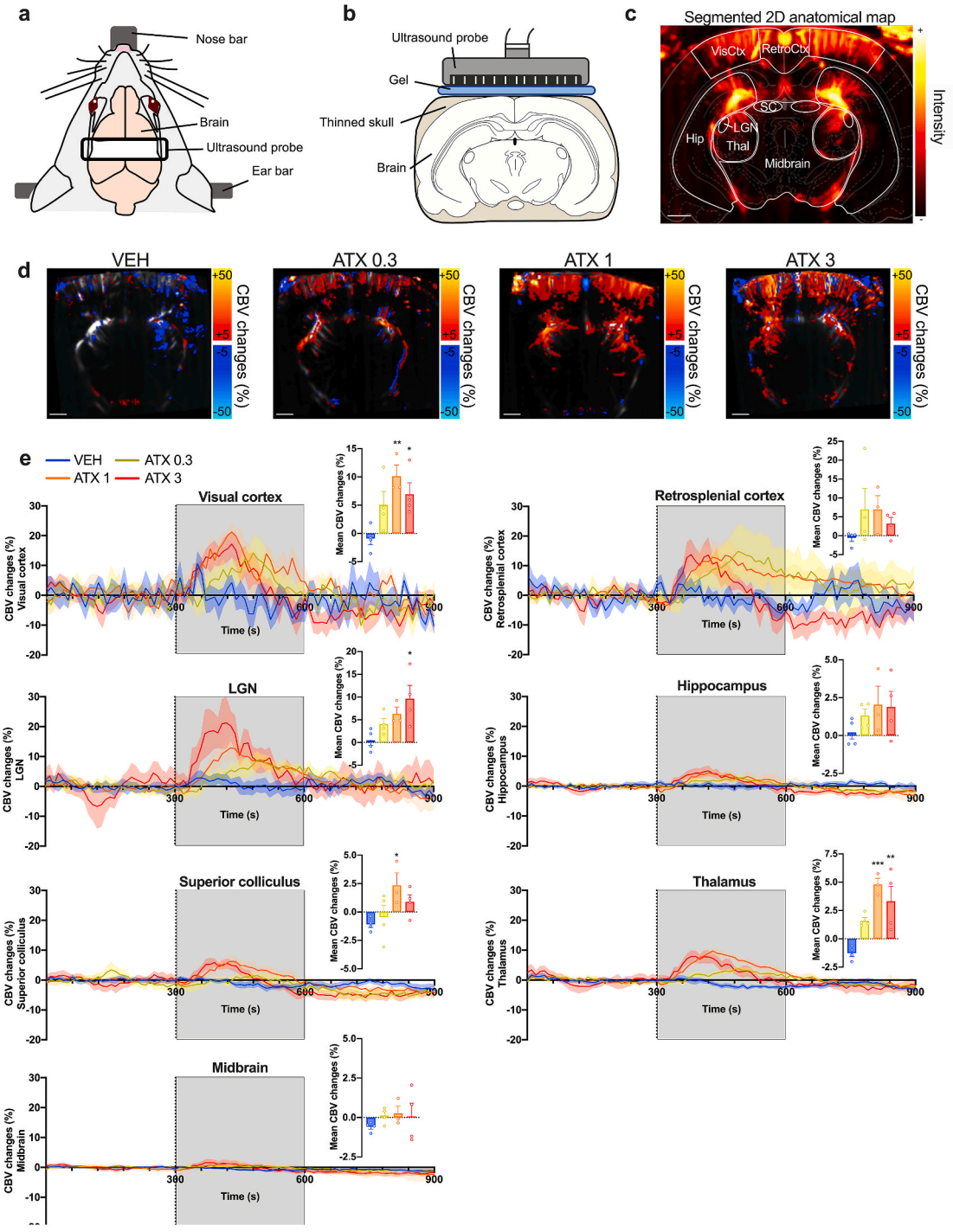

Fig. 1. Pharmaco-fUS imaging of atomoxetine in anesthetized rats. (A) Schematic representation of the experimental setup during fUS imaging. (B) Position of the fUS probe in a coronal brain plan (−5.3 mm from bregma). (C) Typical coronal slice of a rat brain with segmented regions of interest (white) based on the Paxinos and Watson rat brain atlas. (D) Mean CBV changes occurring in single scans during 5 min after injection of VEH (vehicle) or ATX as compared to the baseline signal. (E) Time curves of CBV changes in the different regions of interest (n = 4 rats per group, except n = 3 rats for ATX1; mean curves ± S.E.M). The injection time is shown by a dashed line. Corresponding mean CBV changes during the 0–5 min post-injection period (grey rectangle on the curves) are shown for each region (means ± S.E.M). One ANOVA followed by Dunnett's multiple comparisons test, *p < 0.05; **p < 0.01; ***p < 0.001.

reviewed and non-relevant components were removed (spatial domain outside the brain, scanner-related artefact - see Fig. 3c). As previously, an isotropic Gaussian filter was then applied to the denoised data before the time-bins analysis in SPM12. The first and second-level analyzes were the same as previously.

In the last approach (Fig. 3d), we used the same preprocessing steps, with a different statistical approach to model the effects of atomoxetine. An ICA analysis was performed on the preprocessed data at the group level to identify components of interest from which the time courses could then be used as regressors for general linear modeling. Analysis was carried out using Tensorial Independent Component Analysis (Beckmann and Smith, 2005) as implemented in MELODIC. Pre-processed data were whitened and projected into a 3-dimensional subspace using Principal Component Analysis. Estimated Component

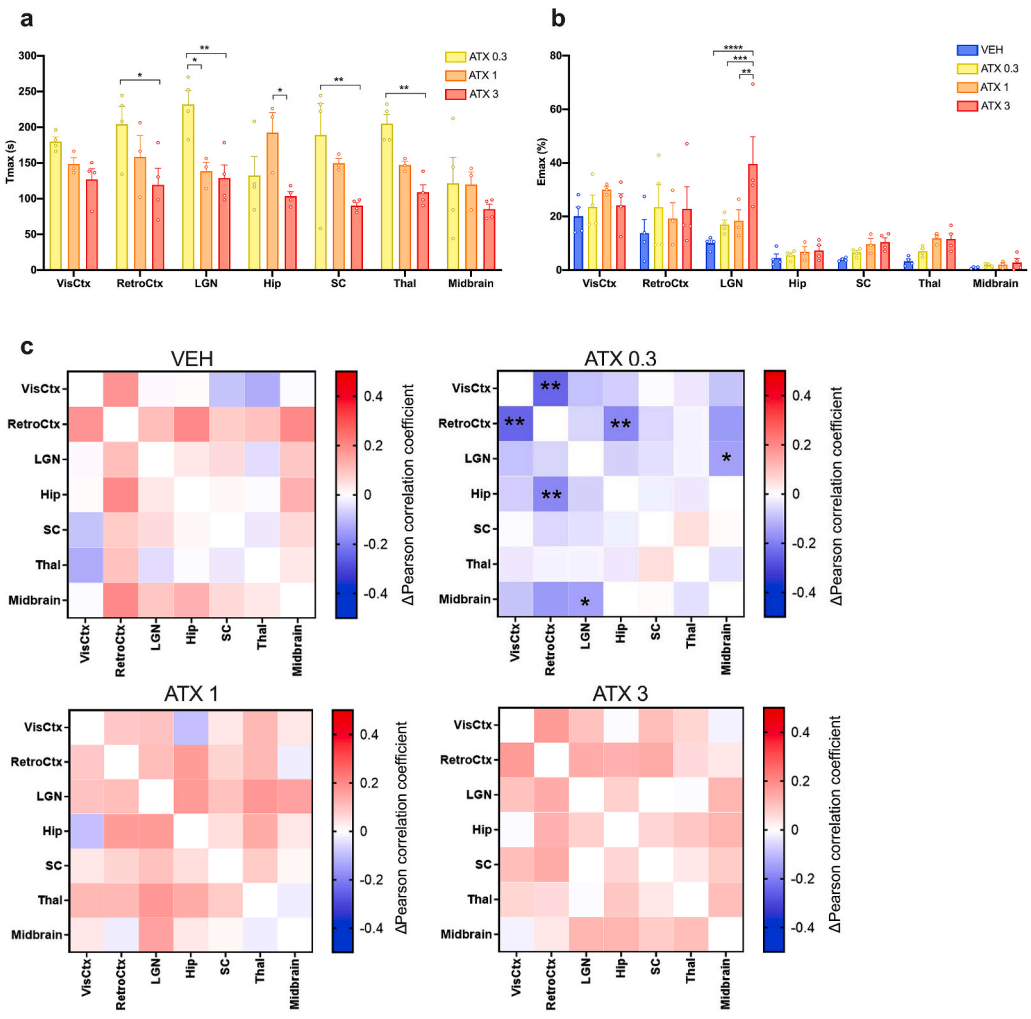

Fig. 2. Time profiles of CBV changes following atomoxetine injection in regions of interest. (A) Time to reach the maximal CBV increases (Tmax) after injection of ATX. Two-way ANOVA followed by Tukey's post-hoc test, *p < 0.05; **p < 0.01. (B) Maximal CBV increases after the pharmacological challenge. Two-way ANOVA followed by Tukey's post-hoc test, **p < 0.01; ***p < 0.001; ****p < 0.0001. (C) Functional connectivity changes after the pharmacological challenge. For each group, matrices of the correlation coefficient variations after injection compared to baseline are shown. For statistical comparisons, a Fisher Z-transformation was applied to the correlation coefficients before two-way ANOVA followed by Dunnett's multiple comparisons test (*p < 0.05; **p < 0.01).

maps were thresholded by fitting a mixture model to the histogram of intensity values (Beckmann and Smith, 2004). Each of the components were then used as regressors for a first-level analysis in FEAT to produce statistical activation maps.

2.5. Statistical analysis

For the analysis of CBV changes in the ROIs, post-injection changes induced by atomoxetine were compared to the saline injection using one-way ANOVA followed by Dunnett's post-hoc tests. Emax and Tmax values were compared between groups using two-way ANOVA with Tukey's post-hoc tests. The statistical significance was set at $p < 0.05$.

For the analysis of functional connectivity, the correlation coefficients were transformed by Fisher Z-transformation to ensure normal distribution. The post-injection changes of correlation coefficients were statistically compared to the saline injection for each dose of atomoxetine using a two-way ANOVA followed by Dunnett's multiple comparisons tests. The statistical significance was set at $p < 0.05$.

For pixel-based analyses, the contrast data obtained in the first-level analyses were used for the second-level analysis in SPM12 using one-way ANOVA for the inter-group comparison. The resulting maps of T-scores were converted into Z-scores and the statistical significance was set at $p < 0.01$.

3. Results

ATX – and not saline - induced widespread increases of CBV after injection, as shown in Fig. 1d with individual maps of raw CBV changes. The hemodynamic effects of ATX were further characterized using region of interest or pixel analyzes.

3.1. Analysis on the regions of interest

The CBV changes induced by ATX were variable across regions (Fig. 1e), with a large impact on the visual cortex and the thalamus, at 1 and 3 mg/kg. A transient increase was also noted in the lateral geniculate nucleus, the only region with CBV changes proportional to the dose. Other regions showed similar time courses but to a less extent, such as the superior colliculus and the hippocampus (Table 1).

Interestingly, we also noticed that the peak of CBV increase (Tmax) was reached faster when increasing the dose, especially in the retrosplenial cortex, the superior colliculus and the thalamus (Fig. 2a). Similarly, Emax was dose-proportional in the lateral geniculate nucleus (Fig. 2b, Table 1).

3.2. Functional connectivity analysis

Functional connectivity was calculated for each group as changes compared to the baseline. Atomoxetine did not induce significant changes in connectivity between the regions of interest at the high doses tested (1 mg/kg and 3 mg/kg), as compared to saline (Fig. 2c). On the contrary, the low dose of atomoxetine globally decreased connectivity, with a significant effect between the retrosplenial cortex and the visual cortex ($p = 0.0066$) or the hippocampus ($p = 0.0054$), and between the

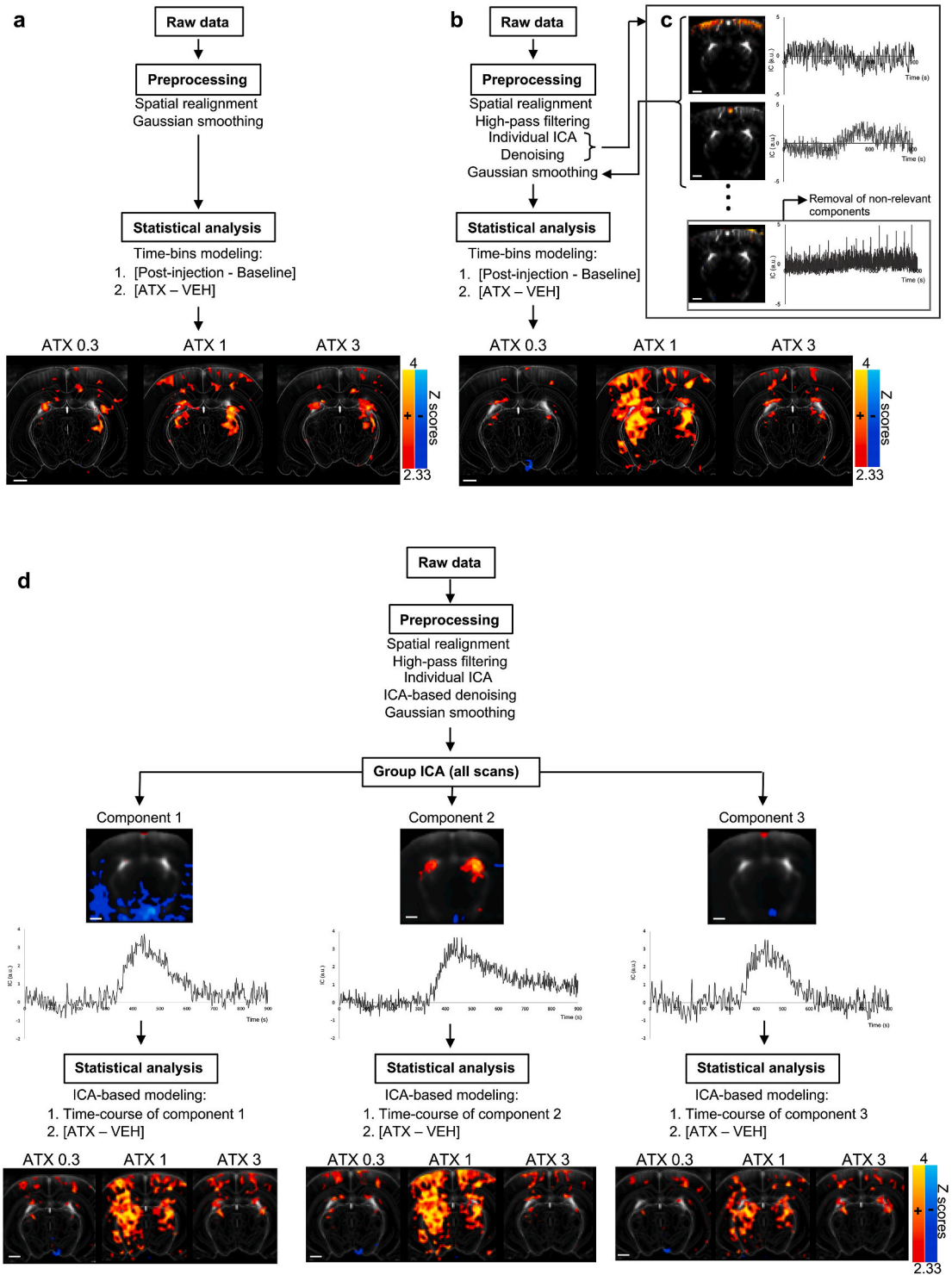

Fig. 3. Pixel-based analyses of CBV changes induced by ATX. (A) Significant CBV changes maps obtained after spatial realignment, smoothing and time-bins statistical comparisons between the first 5 min after the pharmacological challenge and the baseline time-bin, for each dose of ATX versus vehicle ($p < 0.01$). Z scores in color scale (increases in red/yellow, decreases in blue). (B) Significant CBV changes maps obtained after spatial realignment, individual ICA for identification of spatio-temporal components and removal of non-relevant components, smoothing and time-bins statistical comparisons between the first 5 min after the pharmacological challenge and the baseline time-bin, for each dose of ATX versus vehicle ($p < 0.01$). Z scores in color scale (increases in red/yellow, decreases in blue). (C) Example of components identified by an individual ICA. (D) CBV changes maps correlated with different temporal regressors, obtained after spatial realignment, individual ICA for identification of spatio-temporal components and removal of non-relevant components, smoothing and identification of the regressors based on a group ICA analysis for further modeling of the temporal response, for each dose of ATX versus vehicle ($p < 0.01$). Z scores in color scale on the bottom figures. . (For interpretation of the references to color in this figure legend, the reader is referred to the Web version of this article).

Table 1
Mean signal changes after atomoxetine administration in anesthetized rats.

	Treatment		Regions of interest						
			Visual cortex	**Retrosplenial cortex**	**LGN**	**Hip**	**Superior colliculus**	**Thalamus**	**Midbrain**
CBV changes	All	$F_{(3, 11)}$	5,39	1,13	4,3	1,11	3,44	11,1	0,55
		P value	0,016	0,379	0,031	0,387	0,056	0,001	0,656
	ATX 0.3	change %	5,95	7,6	3,59	1,11	0,64	2,85	0,71
		P value	0,117	0,299	0,418	0,627	0,886	0,052	0,635
	ATX 1	change %	11	7,58	5,82	1,84	3,44	6,06	0,85
		P value	**0,008**	0,356	0,151	0,321	**0,034**	**0,001**	0,566
	ATX 3	change %	7,81	3,79	9,15	1,68	1,98	4,58	0,66
		P value	**0,036**	0,767	**0,013**	0,329	0,217	**0,003**	0,678
Tmax	All	$F_{(2, 56)}$	22						
		P value	<0,0001						
	ATX 0.3	Tmax (s)	179,9	204,4	231,9	132,4	189,4	204,9	121,4
	ATX 1	Tmax (s)	148,4	158,4	138,4	192,4	149,7	147,1	119,7
	ATX 3	Tmax (s)	126,9	119,4	128,9	103,4	90,4	108,9	85,4
Emax	All	$F_{(3, 77)}$	6,64						
		P value	0,0005						
	VEH	Emax %	20,1	13,8	10,1	4,53	3,96	3,3	0,92
	ATX 0.3	Emax %	23,6	23,5	16,9	5,55	6,59	7,03	1,79
	ATX 1	Emax %	30	19,2	18,4	6,81	9,65	11,9	2,05
	ATX 3	Emax %	24,2	22,9	39,6	7,37	10,5	11,6	2,85

Note: ATX: atomoxetine; CBV: cerebral blood volume; Hip: hippocampus; LGN: lateral geniculate nuclei; VEH: vehicle.

LGN and the midbrain ($p = 0.0148$).

3.3. Pixel-based analysis

Several approaches were used to characterize the hemodynamic effects of atomoxetine at the pixel level. First, different time-bins were compared on non-denoised and non-filtered data (Fig. 3a). Consistently with the results obtained in the regions of interest analysis, all doses of ATX significantly increased CBV in several areas during the first 5 min compared to saline. Clusters were found within the visual cortex (especially at 1 mg/kg), dentate gyrus, and the thalamus (Fig. 3a).

Secondly, statistical comparisons were made between the different time-bins, after high-pass filtering and exploratory ICA analysis with the pulling out of non-relevant components of the data (Fig. 3b). Subject-level ICA enabled decomposition of the data into a series of spatial components with distinct time courses (Fig. 3c). Results were consistent across the different scans with i) recurrent identification of the left and right visual cortex as one of the first components (top of Fig. 3c), ii) identification of the retrosplenial cortex as a distinct component with a different time profile (middle of Fig. 3c), and iii) other components that were likely related to the drug effects on brain activity given the spatial maps, the low frequency fluctuations and clear signal changes that appeared few minutes after the injection. Similarly, this analysis enabled to identify components that were unlikely related to specific cerebral effects of the drug, as the spatial components were found outside the brain and/or with signal fluctuations unrelated to the time of injection. A typical non-relevant and further removed component is shown in bottom of Fig. 3c, with a spatial component located above the cortex boundaries. This resulted in different statistical maps of hemodynamic effects of ATX as compared to the saline injection (Fig. 3b). Differences between doses are evidenced more precisely, with few activated clusters found with ATX at 0.3 mg/kg in the visual cortex, the hippocampus, the lateral posterior thalamic nucleus and the LGN. The most significant increases of CBV were found at 1 mg/kg of ATX, with large clusters in the visual cortex, the thalamus and the hippocampus. At the dose of 3 mg/kg of ATX, increases of CBV were less widespread.

Thirdly, instead of comparing time-bins, ICA was performed at the group level to identify regressors that could be used to model the effects of ATX using general linear modeling (Fig. 3d). Three components were modelled, they all displayed a rapid increase of CBV, reaching peak between 400 and 500 s. The first component, supporting 44.4% of variance, returned to baseline after 700 s. The second component, (28.3% of variance), showed a slow decrease of CBV that persisted above baseline after 900 s. The third component, (27.3% of variance), was the most transient, with a return to baseline at 600 s.

Each of these components was used as a regressor for the intra-scan general linear modeling and the groups were statistically compared with saline. The maps of CBV changes following these regressors provided more precise and significant effects of ATX compared to the time-bins comparisons, notably regarding the duration of CBV changes across regions (Fig. 3d). At the dose of 0.3 mg/kg, all regressors highlighted a significant effect of ATX in the visual cortex, with larger clusters compared to the time-bins analysis and similar small clusters in the dentate gyrus and thalamus. The maps were similar for the three regressors. At the dose of 1 mg/kg, highly significant activations were found with the three regressors. The second regressor described best the effects of ATX 1 mg/kg, with widespread clusters covering most of the brain. At the dose of 3 mg/kg, maps were similar to those obtained with the time-bins analysis, but effect was more significant in the LGN and more widespread in the cortex. When comparing the different regressors, more transient effects (third regressor) were observed in the LGN and the deeper parts of the cortex, whereas more persistent effects (second regressor) were found in the superficial layers of the medial parts of visual cortex.

4. Discussion

fUS is a new functional neuroimaging technique that relies on plane wave transmission, enabling to capture and average thousands of frames per second to finally obtain Power Doppler images, directly proportional to the cerebral blood volume, of high spatial resolution (about 100 μm). Therefore, fUS allows the monitoring of cerebral activity changes (see Deffieux et al., 2018 for a review). fUS imaging presents several advantages compared to fMRI. First, its spatial and temporal resolution are higher (100 μm and 1s in the current study, compared to typically 300 μm and 2–3 s with fMRI - (Logothetis, 2008)), enabling to detect faster events within smaller clusters, a crucial point in non-clinical imaging considering the limited size of functionally important brain regions in small species such as mice and rats. Secondly, fUS enables a direct measurement of CBV changes, whereas fMRI monitors the Blood-Oxygen-Level-Dependent (BOLD) signal, this latter being a less straightforward index relying on the local concentration of deoxyhemoglobin, which is impacted in opposite ways by CBV changes and local oxygen consumption, both increasing during neuronal activation

(Mandeville et al., 2014). Although it is possible to measure CBV using fMRI, it is necessary to inject iron oxide contrast agents, which can accumulate in tissues if used several times on the same animal, with a compromise that still needs to be made in terms of temporal resolution to achieve a sufficient spatial resolution (Mandeville et al., 2014). Besides, using fUS, it is possible to measure CBV changes in freely-moving animals (see Blaize et al., 2020 and Dizeux et al., 2019 for nonhuman primates, and Sieu et al., 2015 and Urban et al., 2015 for rodents). Despite these advantages, and with the exception of work using local administration (Mace et al., 2011), no study has yet shown the possibility to apply fUS to the neuropharmacology field using systemic administration to monitor acute CBV changes, similarly to pharmacological MRI (Jenkins, 2012).

The aim of this proof-of-concept study was to evaluate the sensitivity of fUS in a pharmacological challenge by ATX. Hence, several methodological approaches have been used. Quantification of signal changes in several region of interests provided important information regarding the spatial and temporal effects of the drug, both in terms of acute effects on CBV and functional connectivity. As the assignment of the ROIs is crucial and can impact the results, complementary pixel-based analyses were reported, to fully characterize the drug effects. We used SPM12 software to realign the different sets of data, enabling statistical comparisons between the different doses of ATX and saline injection. Time-bins comparisons were performed, similarly to pharmacological MRI protocols (McKie et al., 2005; Vidal et al., 2019) and provided high-resolution mapping of CBV changes following ATX injection that was consistent with results of the ROIs analysis. As a further step towards drug characterization, we used ICA to analyze the data without making any assumption on time-bins or temporal regressors. This analysis has been shown as promising for pharmacoMRI studies (Hoff et al., 2010; Mandeville et al., 2014; Rauch et al., 2008). Here, we successfully used ICA for different purposes: individual ICA as a way to identify non-relevant components and remove them from the data, and group ICA to identify temporal regressors for further comparisons between saline and ATX. Conclusively, and as observed across the different analyses, atomoxetine produced a robust CBV increase in different regions of interest, including visual (and retrosplenial) cortex, thalamus and more specifically lateral geniculate nuclei. We also found a CBV increase in the dentate gyrus and a CBV decrease in the ventral tegmental area at low dose of ATX (on the denoised data). Group ICA-based modeling showed local variations in the persistence of CBV increases. These results are unlikely related to possible peripheral effects of ATX, as we found no significant changes in heart or respiratory rates following injection (data not shown). We here show that both time-bins and ICA-based modeling can provide meaningful and complementary information regarding the effect of central drugs; the former is easier to perform but requires an hypothesis regarding the duration of the time-bins, while the latter is entirely exploratory and more informative regarding the time course of drug effects (as shown here by the three different regressors). In addition, ICA can also be used to perform denoising of the data which proves useful to remove artifacts and therefore increase the sensitivity of the analysis, but requires a careful selection of non-relevant components. Conclusively, both pixel and ROIs-based analyses shown that ATX increased CBV mostly in LGN and thalamic structures, and also in cortical areas. The pixel-based analyses also enabled to show a consistent increase in the dentate gyrus at every dose.

NET is expressed in rat thalamus, hippocampus and cortex (Schroeter et al., 2000; Tejani-Butt, 1992). Meanwhile, ATX administration result in an increase of extracellular NE concentration in various cortical and hippocampal areas (Swanson et al., 2006). Coherently, the effects of ATX in our study were focused in the dentate gyrus of the hippocampus, which is consistent with the strong noradrenergic innervation (Pickel et al., 1974) and functional importance of NE in this region (Harley, 2007). Concerning the thalamus, LGN were particularly impacted by ATX. An electrophysiological study performed in anesthetized rats also revealed that ATX (0.5 mg/kg; i.p.) enhanced the responses of the dorsal LGN neurons (Navarra et al., 2013). In addition, ATX also induced CBV increases in the lateral posterior thalamic nuclei, which are also involved in visual stimuli processing (Allen et al., 2016), the superior colliculi and the visual cortex.

Previous studies have already investigated the effect of ATX on brain hemodynamic parameters. Our data are consistent with the pharmacoMRI study by Easton and collaborators that showed positive BOLD changes in lateral posterior thalamic nucleus or dentate gyrus after intraperitoneally acute administration of ATX 2 mg/kg in anesthetized rats (Easton et al., 2007). These regions were found to be among the most significantly impacted at all doses of ATX in the pixel-based analyses, but we were also able to detect additional changes in other thalamic areas and in the visual cortex, potentially explained by the higher sensitivity of fUS. On the contrary, Easton et al. found a relative increase of BOLD signal in the ventral tegmental area (VTA) and the substantia nigra (SN), whereas the results in the ventral midbrain were not consistent in our own study. This may be explained by mixed effects of ATX in these regions, as complex interactions exist between noradrenergic and dopaminergic systems (Avery and Krichmar, 2017). Another clinical study focused on the effect of 60 mg of ATX on the cerebral blood flow (CBF) measured by arterial spin labeling (Marquand et al., 2012). This study showed that ATX decreased CBF in the thalamus and the midbrain. Due to the methodological differences - conscious humans vs. anesthetized rats, CBF vs. CBV, and different result analysis methodologies - these findings are difficult to compare with our own results.

We also evaluated the effects of ATX on functional connectivity. We showed a significant decrease of functional connectivity between retrosplenial cortex and visual cortex or hippocampus at low dose of ATX, and non-significant increases of global connectivity at higher doses. Although the influence of the dose of ATX on connectivity is unclear, a low dose of ATX may induce more subtle changes in NE levels that would be observed only in discrete regions as opposed to a more global and uniform effect at higher doses, which may explain the present findings. Interestingly, a fMRI study in human also showed a decrease of functional connectivity by a single oral dose of atomoxetine, especially involving the visual cortex (van den Brink et al., 2016). The authors interpreted their findings based on the known interaction between NE and glutamate levels (Mather et al., 2016). When there is no incoming sensory information, when glutamate levels are low, NE would decrease functional connectivity, whereas connectivity would be increased by NE during task performance when glutamate levels are higher. This hypothesis is supported by a study using the alpha-2 adrenergic agonist clonidine, that showed a decrease of connectivity at rest whereas clonidine increased connectivity during a task (Coull et al., 1999).

Several conclusions can be driven from this first pharmaco-fUS study. First, our results are consistent with the known effects of atomoxetine on noradrenergic system and previous fMRI and electrophysiological data in terms of regions involved. This is in line with other fUS studies that reported consistency between the measurement of CBV changes and fMRI BOLD changes (Boido et al., 2019) or simultaneous EEG recordings (Bergel et al., 2018; Mace et al., 2011). Secondly, our data also supports the much higher sensitivity of fUS imaging compared to BOLD signal imaging using fMRI in the context of pharmacological challenges. For instance, Easton and colleagues reported a maximal BOLD signal increase of about 1.5–2% in the thalamus (Easton et al., 2007), whereas we found maximal CBV increases that ranged from 7 to 12% in the same region. Our data also brings new information regarding the pronounced effect of atomoxetine in cortical areas, which was not found in the same previous study, and may be very relevant to explain its therapeutic potential in ADHD. Indeed, both visual cortex and retrosplenial/cingulate cortex have been shown to display abnormalities in ADHD (Ahrendts et al., 2011; Vogt, 2019). Although other studies need to confirm the high potential of pharmaco-fUS, it appears therefore as a promising tool for neuropharmacology that will be complementary with

fMRI, especially when there are prior hypotheses regarding the regions of interest that need to be studied.

There are some limitations to our study. We chose to investigate the effect of a single acute dose, similarly to other studies (Easton et al., 2007; Marquand et al., 2012), while efficacy of atomoxetine was reported after several weeks of treatment (Hutchison et al., 2016; Montoya et al., 2009). Our study is therefore a first characterization of acute ATX effects rather than an explanation of the long-term pharmacological and therapeutic effects of the drug. On a similar aspect, we used wild type rats but future studies regarding the therapeutic potential of ATX could focus on relevant models such as spontaneously hypertensive rats for ADHD. Finally, animals were anesthetized and the possibility to explore CBV changes in conscious animals could be the next step in pharmaco-fUS imaging.

In the current study, we confirmed the potential of fUS imaging to characterize dynamic profiles of CNS drugs, in particular ATX, in rats. We reported the high-resolution mapping of CBV changes induced ATX using multiple ROI-based or pixel-based analyses, and application of independent component analysis for data denoising and as a method to model drug hemodynamic effects. Therefore, our study demonstrates that pharmaco-fUS data can be analyzed using the same strategies and softwares that were previously used for pharmacoMRI studies, opening large possibilities for future studies. The high sensitivity and portability of the technique could greatly improve our understanding of hemodynamic profiles of drugs. Therefore, pharmaco-fUS may constitute a new step to move forward in drug development for neurological disorders.

Funding

This work was supported by Theranexus Company.

Author contributions

BV and MV performed the fUS experiments. MD, BV and LV analyzed the data. MD and MC designed the experiments and managed the project. MD, BV and MC wrote the first draft. MD, BV, LZ, FM, MC reviewed the article. All authors approved the final manuscript.

CRediT authorship contribution statement

Benjamin Vidal: Investigation, Formal analysis, Writing - original draft, Writing - review & editing. **Marine Droguerre:** Conceptualization, Formal analysis, Writing - original draft, Writing - review & editing, Project administration. **Ludovic Venet:** Software, Formal analysis. **Luc Zimmer:** Writing - review & editing. **Marco Valdebenito:** Investigation. **Franck Mouthon:** Writing - review & editing. **Mathieu Charvériat:** Conceptualization, Writing - original draft, Writing - review & editing, Supervision.

Declaration of competing interest

MD, BV, LV, FM and MC are full-time employees of Theranexus company. The other authors (LZ and MV) declare no financial conflict of interest.

References

Ahrendts, J., Rusch, N., Wilke, M., Philipsen, A., Eickhoff, S.B., Glauche, V., Perlov, E., Ebert, D., Hennig, J., van Elst, L.T., 2011. Visual cortex abnormalities in adults with ADHD: a structural MRI study. World J. Biol. Psychiatr. 12, 260–270.

Allen, A.E., Procyk, C.A., Howarth, M., Walmsley, L., Brown, T.M., 2016. Visual input to the mouse lateral posterior and posterior thalamic nuclei: photoreceptive origins and retinotopic order. J. Physiol. 594, 1911–1929.

Arime, Y., Kubo, Y., Sora, I., 2011. Animal models of attention-deficit/hyperactivity disorder. Biol. Pharm. Bull. 34, 1373–1376.

Avery, M.C., Krichmar, J.L., 2017. Neuromodulatory systems and their interactions: a review of models, theories, and experiments. Front. Neural Circ. 11, 108.

Beckmann, C.F., Smith, S.M., 2004. Probabilistic independent component analysis for functional magnetic resonance imaging. IEEE Trans. Med. Imag. 23, 137–152.

Beckmann, C.F., Smith, S.M., 2005. Tensorial extensions of independent component analysis for multisubject FMRI analysis. Neuroimage 25, 294–311.

Bercoff, J., Montaldo, G., Loupas, T., Savery, D., Meziere, F., Fink, M., Tanter, M., 2011. Ultrafast compound Doppler imaging: providing full blood flow characterization. IEEE Trans. Ultrason. Ferroelectrics Freq. Contr. 58, 134–147.

Bergel, A., Deffieux, T., Demene, C., Tanter, M., Cohen, I., 2018. Local hippocampal fast gamma rhythms precede brain-wide hyperemic patterns during spontaneous rodent REM sleep. Nat. Commun. 9, 5364.

Bimbard, C., Demene, C., Girard, C., Radtke-Schuller, S., Shamma, S., Tanter, M., Boubenec, Y., 2018. Multi-scale mapping along the auditory hierarchy using high-resolution functional UltraSound in the awake ferret. Elife 7.

Blaize, K., Arcizet, F., Gesnik, M., Ahnine, H., Ferrari, U., Deffieux, T., Pouget, P., Chavane, F., Fink, M., Sahel, J.A., Tanter, M., Picaud, S., 2020. Functional ultrasound imaging of deep visual cortex in awake nonhuman primates. Proc. Natl. Acad. Sci. U. S. A. 117, 14453–14463.

Boido, D., Rungta, R.L., Osmanski, B.F., Roche, M., Tsurugizawa, T., Le Bihan, D., Ciobanu, L., Charpak, S., 2019. Mesoscopic and microscopic imaging of sensory responses in the same animal. Nat. Commun. 10, 1110.

Brown, T.E., Holdnack, J., Saylor, K., Adler, L., Spencer, T., Williams, D.W., Padival, A. K., Schuh, K., Trzepacz, P.T., Kelsey, D., 2011. Effect of atomoxetine on executive function impairments in adults with ADHD. J. Atten. Disord. 15, 130–138.

Bymaster, F.P., Katner, J.S., Nelson, D.L., Hemrick-Luecke, S.K., Threlkeld, P.G., Heiligenstein, J.H., Morin, S.M., Gehlert, D.R., Perry, K.W., 2002. Atomoxetine increases extracellular levels of norepinephrine and dopamine in prefrontal cortex of rat: a potential mechanism for efficacy in attention deficit/hyperactivity disorder. Neuropsychopharmacology 27, 699–711.

Catana, C., 2019. Development of dedicated brain PET imaging devices: recent advances and future perspectives. J. Nucl. Med. 60, 1044–1052.

Coull, J.T., Buchel, C., Friston, K.J., Frith, C.D., 1999. Noradrenergically mediated plasticity in a human attentional neuronal network. Neuroimage 10, 705–715.

Cubillo, A., Smith, A.B., Barrett, N., Giampietro, V., Brammer, M.J., Simmons, A., Rubia, K., 2014. Shared and drug-specific effects of atomoxetine and methylphenidate on inhibitory brain dysfunction in medication-naive ADHD boys. Cerebr. Cortex 24, 174–185.

Deffieux, T., Demene, C., Pernot, M., Tanter, M., 2018. Functional ultrasound neuroimaging: a review of the preclinical and clinical state of the art. Curr. Opin. Neurobiol. 50, 128–135.

Demene, C., Baranger, J., Bernal, M., Delanoe, C., Auvin, S., Biran, V., Alison, M., Mairesse, J., Harribaud, E., Pernot, M., Tanter, M., Baud, O., 2017. Functional ultrasound imaging of brain activity in human newborns. Sci. Transl. Med. 9.

Demene, C., Deffieux, T., Pernot, M., Osmanski, B.F., Biran, V., Gennisson, J.L., Sieu, L. A., Bergel, A., Franqui, S., Correas, J.M., Cohen, I., Baud, O., Tanter, M., 2015. Spatiotemporal clutter filtering of Ultrafast ultrasound data highly increases Doppler and fUltrasound sensitivity. IEEE Trans. Med. Imag. 34, 2271–2285.

Dizeux, A., Gesnik, M., Ahnine, H., Blaize, K., Arcizet, F., Picaud, S., Sahel, J.A., Deffieux, T., Pouget, P., Tanter, M., 2019. Functional ultrasound imaging of the brain reveals propagation of task-related brain activity in behaving primates. Nat. Commun. 10, 1400.

Easton, N., Marshall, F., Fone, K., Marsden, C., 2007. Atomoxetine produces changes in cortico-basal thalamic loop circuits: assessed by phMRI BOLD contrast. Neuropharmacology 52, 812–826.

Fernando, A.B., Economidou, D., Theobald, D.E., Zou, M.F., Newman, A.H., Spoelder, M., Caprioli, D., Moreno, M., Hipolito, L., Aspinall, A.T., Robbins, T.W., Dalley, J.W., 2012. Modulation of high impulsivity and attentional performance in rats by selective direct and indirect dopaminergic and noradrenergic receptor agonists. Psychopharmacology (Berlin) 219, 341–352.

Gau, S.S., Shang, C.Y., 2010. Improvement of executive functions in boys with attention deficit hyperactivity disorder: an open-label follow-up study with once-daily atomoxetine. Int. J. Neuropsychopharmacol. 13, 243–256.

Gehlert, D.R., Schober, D.A., Hemrick-Luecke, S.K., Krushinski, J., Howbert, J.J., Robertson, D.W., Fuller, R.W., Wong, D.T., 1995. Novel halogenated analogs of tomoxetine that are potent and selective inhibitors of norepinephrine uptake in brain. Neurochem. Int. 26, 47–52.

Gesnik, M., Blaize, K., Deffieux, T., Gennisson, J.L., Sahel, J.A., Fink, M., Picaud, S., Tanter, M., 2017. 3D functional ultrasound imaging of the cerebral visual system in rodents. Neuroimage 149, 267–274.

Harley, C.W., 2007. Norepinephrine and the dentate gyrus. Prog. Brain Res. 163, 299–318.

Hoff, E.I., van Oostenbrugge, R.J., Otte, W.M., van der Marel, K., Steinbusch, H.W., Dijkhuizen, R.M., 2010. Pharmacological magnetic resonance imaging of muscarinic acetylcholine receptor activation in rat brain. Neuropharmacology 58, 1252–1257.

Hutchison, S.L., Ghuman, J.K., Ghuman, H.S., Karpov, I., Schuster, J.M., 2016. Efficacy of atomoxetine in the treatment of attention-deficit hyperactivity disorder in patients with common comorbidities in children, adolescents and adults: a review. Ther Adv Psychopharmacol 6, 317–334.

Hyvarinen, A., 1999. Fast and robust fixed-point algorithms for independent component analysis. IEEE Trans. Neural Network. 10, 626–634.

Imbault, M., Chauvet, D., Gennisson, J.L., Capelle, L., Tanter, M., 2017. Intraoperative functional ultrasound imaging of human brain activity. Sci. Rep. 7, 7304.

Jenkins, B.G., 2012. Pharmacologic magnetic resonance imaging (phMRI): imaging drug action in the brain. Neuroimage 62, 1072–1085.

Kohlhauer, M., Lidouren, F., Remy-Jouet, I., Mongardon, N., Adam, C., Bruneval, P., Hocini, H., Levy, Y., Blengio, F., Carli, P., Vivien, B., Ricard, J.D., Micheau, P., Walti, H., Nadeau, M., Robert, R., Richard, V., Mulder, P., Maresca, D., Demene, C.,

Pernot, M., Tanter, M., Ghaleh, B., Berdeaux, A., Tissier, R., 2015. Hypothermic total liquid ventilation is highly protective through cerebral hemodynamic preservation and sepsis-like mitigation after asphyxial cardiac arrest. Crit. Care Med. 43, e420–430.
Lancelot, S., Zimmer, L., 2010. Small-animal positron emission tomography as a tool for neuropharmacology. Trends Pharmacol. Sci. 31, 411–417.
Logothetis, N.K., 2008. What we can do and what we cannot do with fMRI. Nature 453, 869–878.
Mace, E., Montaldo, G., Cohen, I., Baulac, M., Fink, M., Tanter, M., 2011. Functional ultrasound imaging of the brain. Nat. Methods 8, 662–664.
Mace, E., Montaldo, G., Trenholm, S., Cowan, C., Brignall, A., Urban, A., Roska, B., 2018. Whole-brain functional ultrasound imaging reveals brain modules for visuomotor integration. Neuron 100, 1241–1251 e1247.
Mandeville, J.B., Liu, C.H., Vanduffel, W., Marota, J.J., Jenkins, B.G., 2014. Data collection and analysis strategies for phMRI. Neuropharmacology 84, 65–78.
Mandino, F., Cerri, D.H., Garin, C.M., Straathof, M., van Tilborg, G.A.F., Chakravarty, M. M., Dhenain, M., Dijkhuizen, R.M., Gozzi, A., Hess, A., Keilholz, S.D., Lerch, J.P., Shih, Y.I., Grandjean, J., 2019. Animal functional magnetic resonance imaging: trends and path toward standardization. Front. Neuroinf. 13, 78.
Marquand, A.F., O'Daly, O.G., De Simoni, S., Alsop, D.C., Maguire, R.P., Williams, S.C., Zelaya, F.O., Mehta, M.A., 2012. Dissociable effects of methylphenidate, atomoxetine and placebo on regional cerebral blood flow in healthy volunteers at rest: a multi-class pattern recognition approach. Neuroimage 60, 1015–1024.
Mather, M., Clewett, D., Sakaki, M., Harley, C.W., 2016. Norepinephrine ignites local hotspots of neuronal excitation: how arousal amplifies selectivity in perception and memory. Behav. Brain Sci. 39, e200.
McKie, S., Del-Ben, C., Elliott, R., Williams, S., del Vai, N., Anderson, I., Deakin, J.F., 2005. Neuronal effects of acute citalopram detected by pharmacoMRI. Psychopharmacology (Berlin) 180, 680–686.
Montaldo, G., Tanter, M., Bercoff, J., Benech, N., Fink, M., 2009. Coherent plane-wave compounding for very high frame rate ultrasonography and transient elastography. IEEE Trans. Ultrason. Ferroelectrics Freq. Contr. 56, 489–506.
Montoya, A., Hervas, A., Cardo, E., Artigas, J., Mardomingo, M.J., Alda, J.A., Gastaminza, X., Garcia-Polavieja, M.J., Gilaberte, I., Escobar, R., 2009. Evaluation of atomoxetine for first-line treatment of newly diagnosed, treatment-naive children and adolescents with attention deficit/hyperactivity disorder. Curr. Med. Res. Opin. 25, 2745–2754.
Navarra, R.L., Clark, B.D., Zitnik, G.A., Waterhouse, B.D., 2013. Methylphenidate and atomoxetine enhance sensory-evoked neuronal activity in the visual thalamus of male rats. Exp. Clin. Psychopharmacol 21, 363–374.
Osmanski, B.F., Martin, C., Montaldo, G., Laniece, P., Pain, F., Tanter, M., Gurden, H., 2014. Functional ultrasound imaging reveals different odor-evoked patterns of vascular activity in the main olfactory bulb and the anterior piriform cortex. Neuroimage 95, 176–184.
Paxinos, G., Watson, C., 1998. A Stereotaxic Atlas of the Rat Brain. Academic, New York.
Pickel, V.M., Segal, M., Bloom, F.E., 1974. A radioautographic study of the efferent pathways of the nucleus locus coeruleus. J. Comp. Neurol. 155, 15–42.
Pliszka, S.R., 2003. Non-stimulant treatment of attention-deficit/hyperactivity disorder. CNS Spectr. 8, 253–258.
Rau, R., Kruizinga, P., Mastik, F., Belau, M., de Jong, N., Bosch, J.G., Scheffer, W., Maret, G., 2018. 3D functional ultrasound imaging of pigeons. Neuroimage 183, 469–477.
Rauch, A., Rainer, G., Augath, M., Oeltermann, A., Logothetis, N.K., 2008. Pharmacological MRI combined with electrophysiology in non-human primates: effects of Lidocaine on primary visual cortex. Neuroimage 40, 590–600.
Schroeter, S., Apparsundaram, S., Wiley, R.G., Miner, L.H., Sesack, S.R., Blakely, R.D., 2000. Immunolocalization of the cocaine- and antidepressant-sensitive l-norepinephrine transporter. J. Comp. Neurol. 420, 211–232.
Sieu, L.A., Bergel, A., Tiran, E., Deffieux, T., Pernot, M., Gennisson, J.L., Tanter, M., Cohen, I., 2015. EEG and functional ultrasound imaging in mobile rats. Nat. Methods 12, 831–834.
Swanson, C.J., Perry, K.W., Koch-Krueger, S., Katner, J., Svensson, K.A., Bymaster, F.P., 2006. Effect of the attention deficit/hyperactivity disorder drug atomoxetine on extracellular concentrations of norepinephrine and dopamine in several brain regions of the rat. Neuropharmacology 50, 755–760.
Tatsumi, M., Groshan, K., Blakely, R.D., Richelson, E., 1997. Pharmacological profile of antidepressants and related compounds at human monoamine transporters. Eur. J. Pharmacol. 340, 249–258.
Tejani-Butt, S.M., 1992. [3H]nisoxetine: a radioligand for quantitation of norepinephrine uptake sites by autoradiography or by homogenate binding. J. Pharmacol. Exp. Therapeut. 260, 427–436.
Tiran, E., Ferrier, J., Deffieux, T., Gennisson, J.L., Pezet, S., Lenkei, Z., Tanter, M., 2017. Transcranial functional ultrasound imaging in freely moving awake mice and anesthetized young rats without contrast agent. Ultrasound Med. Biol. 43, 1679–1689.
Urban, A., Dussaux, C., Martel, G., Brunner, C., Mace, E., Montaldo, G., 2015. Real-time imaging of brain activity in freely moving rats using functional ultrasound. Nat. Methods 12, 873–878.
Urban, A., Golgher, L., Brunner, C., Gdalyahu, A., Har-Gil, H., Kain, D., Montaldo, G., Sironi, L., Blinder, P., 2017. Understanding the neurovascular unit at multiple scales: advantages and limitations of multi-photon and functional ultrasound imaging. Adv. Drug Deliv. Rev. 119, 73–100.
Urban, A., Mace, E., Brunner, C., Heidmann, M., Rossier, J., Montaldo, G., 2014. Chronic assessment of cerebral hemodynamics during rat forepaw electrical stimulation using functional ultrasound imaging. Neuroimage 101, 138–149.
van den Brink, R.L., Pfeffer, T., Warren, C.M., Murphy, P.R., Tona, K.D., van der Wee, N. J., Giltay, E., van Noorden, M.S., Rombouts, S.A., Donner, T.H., Nieuwenhuis, S., 2016. Catecholaminergic neuromodulation shapes intrinsic MRI functional connectivity in the human brain. J. Neurosci. 36, 7865–7876.
Vidal, B., Bolbos, R., Redoute, J., Langlois, J.B., Costes, N., Newman-Tancredi, A., Zimmer, L., 2019. Pharmacological MRI to investigate the functional selectivity of 5-HT1A receptor biased agonists. Neuropharmacology 172, 107867.
Vogt, B.A., 2019. Cingulate impairments in ADHD: comorbidities, connections, and treatment. Handb. Clin. Neurol. 166, 297–314.
Walker, D.J., Mason, O., Clemow, D.B., Day, K.A., 2015. Atomoxetine treatment in adults with attention-deficit/hyperactivity disorder. Postgrad. Med. 127, 686–701.